Investigations of the Myoglobin Cavity Mutant H93G with Unnatural Imidazole Proximal Ligands as a Modular Peroxide O−O Bond Cleavage Model System†

Mark P. Roach,‡ Shin-ichi Ozaki,‡,§ and Yoshihito Watanabe*,‡,||

Institute for Molecular Science, Myodaiji-cho, Okazaki 444-8585, Japan, and Department of Structural Molecular Science, Graduate University for Advanced Studies, Myodaiji-cho, Okazaki 444-8585, Japan

Received September 1, 1999; Revised Manuscript Received November 10, 1999

ABSTRACT: A general inability to elucidate extensive variations in the electronic characteristics of proximal heme iron ligands in heme proteins has hampered efforts to obtain a clear understanding of the role of the proximal heme iron ligand in the activation of oxygen and peroxide. The disadvantage of the frequently applied site-directed mutagenesis technique is that it is limited by the range of natural ligands available within the genetic code. The myoglobin cavity mutant H93G [Barrick, D. (1994) *Biochemistry 33*, 6546−6554] has its proximal histidine ligand replaced with glycine, a mutation which leaves an open cavity capable of accommodating a variety of unnatural potential proximal ligands. We have carried out investigations of the effect of changing the electron donor characteristics of a variety of substituted imidazole proximal ligands on the rate of formation of myoglobin compound II and identified a correlation between the substituted imidazole N-3 pK_a (which provides a measure of the electron donor ability of N-3) and the apparent rate of formation of compound II. A similar rate dependence correlation is not observed upon binding of azide. This finding indicates that O−O bond cleavage and not the preceding peroxide binding step is being influenced by the electron donor characteristics of the substituted imidazole ligands. The proximal ligand effects are clearly visible, but their overall magnitude is quite low (1.7-fold increase in the O−O bond cleavage rate per pK_a unit). This appears to provide support for recent commentaries which concluded that the partial ionization of the proximal histidine ligand in typical heme peroxidases may not be enough of an influence to provide a mechanistically critical push effect [Poulos, T. L. (1996) *JBIC, J. Biol. Inorg. Chem. 1*, 356−359]. Further attempts were made to define the mechanism of the influence of N-3 pK_a on O−O bond cleavage by using peracetic acid and cumene hydroperoxide as mechanistic probes. The observation of heme destruction in these reactions indicates that displacement of the proximal imidazole ligands by peracetic acid or cumene hydroperoxide has occurred. A combination mutation (H64D/H93G) was prepared with the objective of observing compound I of H64D/H93G with substituted imidazoles as proximal ligands upon reaction with H_2O_2. This double mutant was found to simultaneously bind imidazole to both axial positions, an arrangement which prevents a reaction with H_2O_2.

INTRODUCTION

For heme enzymes responsible for activation of oxygen and H_2O_2, the role of the proximal heme iron ligand in the production of oxo−ferryl catalytic heme species remains poorly understood. The "push effect" of the cysteine thiolate ligand has long been proposed to be primarily responsible for efficient heterolysis of peroxide bound trans to the thiolate ligand in the reaction cycle of the cytochrome P450 monooxygenases in the species directly preceding the proposed oxo−ferryl reactive intermediate (*1*−*6*). In typical heme-containing peroxidases, a partially ionized proximal histidine ligand (formed through strong hydrogen bonding of the histidine N-1 to a carboxylate) is a highly conserved structural feature. This has been suggested to be an important structural contribution to the general peroxidase function of efficiently producing a highly oxidizing oxo−ferryl catalytic species (compound I) through an enhanced push effect (*2*−*4*, *6*, *7*). Some of the most important previous advances in studies of the push effect have come both from proximal ligand substitution by site-directed mutagenesis of heme proteins where the proximal histidine ligand of human myoglobin has been converted to cysteine (*8*−*10*) and from thiolate-tethered synthetic iron porphyrin model systems (*11*, *12*). Both of these approaches have shown unequivocally that cysteinate/thiolate proximal heme iron ligation enhances the percentage and rate of heterolysis of peroxides relative to those with histidine/imidazole proximal heme iron ligation. However, directly testing more subtle variations of the histidine ligand which can arise from its interactions with the proximal protein environment is considerably more

† M.P.R. is a Japan Society for the Promotion of Science (JSPS) Postdoctoral Fellow. This work was supported by a Grant-in-Aid for Scientific Research (10680575) to S.O., a JSPS Grant in Aid (97371) to M.P.R., and a JSPS Grant in Aid for Priority Areas, Molecular Biometallics, to Y.W.

* To whom correspondence should be addressed. E-mail: yoshi@ims.ac.jp.

‡ Institute for Molecular Science.

§ Current address: Faculty of Education, Yamagata University, Kojirakawa, Yamagata 990-8560, Japan.

|| Graduate University for Advanced Studies.

10.1021/bi992054v CCC: $19.00
Published on Web 01/22/2000

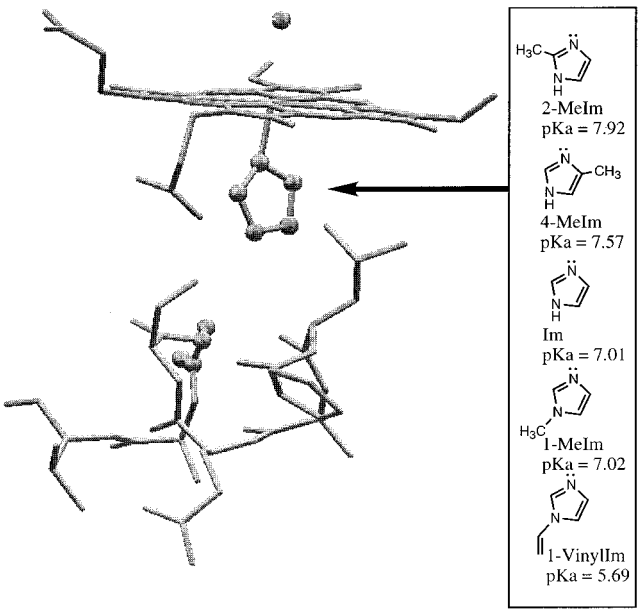

FIGURE 1: Active site of the ferric imidazole adduct of H93G Mb [prepared using InsightII with the H93G structure from the Brookhaven Protein Data Bank (entry 1IRC)]. Glycine 93, imidazole, and the oxygen of the distal water ligand are shown as ball-and-stick representations. Also shown are the five Im-X species used as proximal ligands for H93G and their pK_a values.

challenging. This strategy has been addressed by Morishima, Watanabe, and co-workers, who have shown that when substituted imidazoles are introduced to five-coordinate acylperoxoiron(III) porphyrins at low temperatures, the partitioning of the acylperoxo O−O bond cleavage between heterolysis and homolysis is directly influenced by the electron donor character of the substituted imidazole (*13*). Studies of this effect under biologically relevant conditions, i.e., within a protein environment near ambient temperature in an aqueous medium, are of definite interest. However, a general inability to elucidate extensive variations in the electronic characteristics of proximal heme iron ligands for the purpose of peroxide reactivity studies in proteins has thus far proven to be somewhat of a problem. The disadvantage of the frequently applied site-directed mutagenesis technique is that it is limited by the range of natural ligands available within the genetic code.

Recently, a relatively new class of site-directed mutants has been produced for a number of heme proteins where the amino acid residue bearing the natural heme iron ligand is replaced with a smaller noncoordinating residue. The mutation creates a cavity which can accommodate various exogenous molecules and is thus known as a "cavity mutant". This was first accomplished in the preparation of sperm whale myoglobin (Mb)[1] H93G (Figure 1) by Barrick (*14*, *15*) and has since been extended to the preparation of cytochrome *c* peroxidase H175G (*16*, *17*), heme oxygenase H25A (*18*), and horseradish peroxidase H170A (*19*). The majority of studies involving cavity mutants and unnatural proximal ligands have been carried out on H93G Mb by Boxer and co-workers, who were the first researchers to recognize the utility of the H93G cavity mutant system for studying the effects of unnatural proximal ligands on important properties of heme proteins such as binding of CO and NO (*20*−*24*). The ferric aquo H93G−imidazole adduct has been well characterized by X-ray crystallography (*14*), and cyanoferric H93G-substituted imidazole ligand adducts have been characterized by NMR spectroscopy (*21*). These imidazole adducts of ferric H93G have six-coordinate heme iron coordination structures similar to those of the analogous species of wild-type Mb.

The ability to conveniently alter the electronic properties of the proximal ligand of H93G makes it an ideal system with which to probe the influence of the proximal heme iron ligand on the activation of heme iron-bound peroxide. To our knowledge, this work provides the first example of a systematic study of the effect of variations in the electron donating capability of a proximal heme iron ligand on the rate of reaction of the heme complex with H_2O_2 within a heme protein. The reaction of Mb with H_2O_2 yields Mb-II (also known as oxo−ferryl Mb or compound II) as a relatively stable complex. There are two possible routes to Mb-II following the binding of H_2O_2 to ferric Mb: (i) homolysis of the O−O bond and (ii) heterolysis of the O−O bond to yield an oxo−ferryl porphyrin cation radical species (such as the compound I species observed in the reaction cycle of heme peroxidases) followed by a one-electron reduction of the porphyrin cation radical (Scheme 1). The quenching of the porphyrin cation radical occurs much too quickly for compound I to be observed; thus, the overall observed process is a decay of ferric Mb to Mb-II. When the imidazole adduct of ferric H93G reacts with H_2O_2, a compound II [H93G(Im)-II] species is formed whose magnetic circular dichroism and UV−visible spectra are essentially identical to those of wild-type myoglobin (*25*). This indicates that the proximal ligand tether to the protein is not required for the reaction with H_2O_2 to occur and for a stable compound II to be formed. The Mb cavity mutant H93G is thus a competent system with which to investigate the effects of electronic variations in ligand donor characteristics on O−O bond cleavage.

This work describes our investigations of the role of the proximal heme iron ligand in the activation of peroxide. We have prepared substituted imidazole (Im-X) adducts of ferric H93G and examined their effects on reactions with H_2O_2 and other oxo−ferryl heme-generating oxidants. In addition to the information that becomes available regarding the push effect, this work also represents a significant test of the protein cavity complementation/catalytic rescue strategy which has recently been investigated by Barrick, Boxer, Goodin, Ortiz de Montellano, and their respective co-workers (*15*−*23*).

EXPERIMENTAL PROCEDURES

Preparation of the Myoglobin Mutants. The H93G and H64D/H93G sperm whale myoglobin mutants were constructed from the DNA encoding the original wild-type sperm

[1] Abbreviations: Mb, myoglobin; H93G, histidine 93 to glycine mutant; H64D/H93G, histidine 64 to aspartate and histidine 93 to glycine double mutant; H25A, histidine 25 to alanine mutant; H170A, histidine 170 to alanine mutant; H175G, histidine 175 to glycine mutant; Mb-II, oxo−ferryl myoglobin (or myoglobin compound II); Im-X, substituted imidazoles, including 2-methylimidzole (2-MeIm), 4-methylimidzole (4-MeIm), 1-methylimidazole (1-MeIm), imidazole (Im), and 1-vinylimidazole (1-VinylIm); H93G(Im-X)-II, oxo−ferryl H93G with Im-X as the proximal ligand [or H93G(Im-X) compound II]; H93G(Im-X)-N_3, azide adduct of H93G(Im-X); PAA, peracetic acid; CHP, cumene hydroperoxide.

Scheme 1

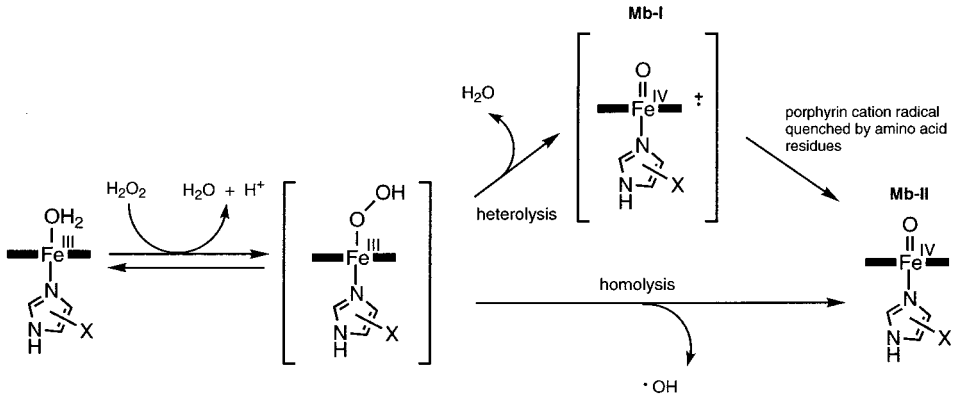

whale myoglobin *Escherichia coli* expression system [which was a gift from J. S. Olson (Rice University, Houston, TX)] by a PCR-based cassette mutagenesis technique. The mutant myoglobins were purified by previously established methods (*14*). The exogenous ligand free form of the mutant myoglobins was prepared by 2-butanone heme extraction according to the method of Teale (*26*) followed by reconstitution of the apo-H93G by addition of 1 equiv of hemin (Wako, Osaka, Japan) from a solution of hemin in 0.1 N NaOH. Sodium phosphate buffer (pH 7.0) was then added to a concentration of 50 mM. The concentration of exogenous ligand free ferric H93G at pH 7.0 was determined from the Soret molar absorptivity value of 115 mM^{-1} cm^{-1} (*27*).

Preparation of H93G(Im-X) Adducts. The substituted imidazole (Im-X) adducts of ferric H93G studied in detail in this work have been prepared from the following: 2-methylimidazole (2-MeIm), 4-methylimidazole (4-MeIm), 1-methylimidazole (1-MeIm), imidazole (Im), and 1-vinylimidazole (1-VinylIm). All Im-X compounds were purchased from Aldrich (Milwaukee, WI), Wako, or Nacalai Tesque (Kyoto, Japan) and used without further purification. Im-X adducts were prepared by addition of concentrated solutions (0.1−1.0 M) of Im-X in either DMSO or 50 mM sodium phosphate buffer (pH 7.0) to exogenous ligand free ferric H93G. Dissociation constants (K_d) for each ligand binding to ferric exogenous ligand free H93G were determined by UV−visible spectroscopic titrations of 5 μM ferric H93G in 50 mM sodium phosphate buffer (pH 7.0) with concentrated solutions (0.1−1.0 M) of Im-X in DMSO (DMSO itself has no effect on the spectrum of exogenous ligand free ferric H93G, whereas ethanol and methanol do cause some spectral changes). The UV−visible spectra were recorded at 25 °C on a Shimadzu UV 2400 spectrophotometer (Shimadzu, Ise, Japan). The data thus obtained were subjected to Hill analyses for the K_d determinations.

Determination of Im-X pK_a Values. The pK_a values for all of the Im-X compounds were determined experimentally by pH titrations of 5 mmol samples with 1 M HCl. All substituted imidazole ligands were first dissolved in DMSO prior to addition to aqueous solution. The final DMSO concentration in all cases was 5%. The final pK_a value was calculated from the average of three determinations.

Reactions of H93G(Im-X) with H_2O_2 To Form H93G(Im-X)-II. The 5 μM samples of ferric H93G in 50 mM sodium phosphate buffer containing Im-X at concentration levels that are 10-fold higher than the K_d for each Im-X were mixed in a 1:1 ratio with various concentrations of H_2O_2 (Kanto Chemical Industries, Tokyo, Japan) (30−120 mM) in the same buffer. Spectra were recorded at 4 °C using a Hi-Tech SF-43 stopped flow apparatus equipped with a MG 6000 diode array spectrophotometer (Hi Tech Ltd., Salisbury, U.K.). Data obtained from the decay of absorbance at 409 nm in the reaction were fitted to a single-exponential equation to obtain k_{obs}[H93G(Im-X)-II], the observed first-order rates of formation of H93G(Im-X)-II. The apparent rates of reaction [k_{app}[H93G(Im-X)-II]] for each Im-X in the series were determined from the slope of a plot of k_{obs}[H93G(Im-X)-II] versus H_2O_2 concentration.

Measurement of Association Rates of H93G(Im-X) with NaN_3. The 10 μM samples of ferric H93G in 50 mM sodium phosphate buffer containing Im-X at concentration levels that are 10-fold higher than the K_d for each Im-X were mixed in a 1:1 ratio with various concentrations of NaN_3 (1−15 mM) in the same buffer. Data collection was carried out with the Hi-Tech stopped flow apparatus described above. The rates of N_3^- association were determined from the decay of the Soret band at 409 nm. The data were fitted to a single-exponential equation to obtain k_{obs}[H93G(Im-X)-N_3], the observed pseudo-first-order rates of association of N_3^- with H93G(Im-X). The apparent rates of reaction [k_{app}[H93G(Im-X)-N_3]] for each Im-X in the series were determined from the slope of a plot of k_{obs}[H93G(Im-X)-N_3] versus NaN_3 concentration.

Measurements of the Soret Bleaching Rates of H93G(Im-X) upon Reaction with Peracetic Acid and Cumene Hydroperoxide. The 10 μM samples of ferric H93G in 50 mM sodium phosphate buffer containing Im-X at concentration levels that are 10-fold higher than the K_d for each Im-X were mixed in a 1:1 ratio with 1 mM peracetic acid (Aldrich) or cumene hydroperoxide (Aldrich) in the same buffer. Data collection was carried out with the Hi-Tech stopped flow apparatus described above. The rates of decay of the Soret band at 409 nm were fitted to a double-exponential equation to obtain k_1, the rate of the first phase of Soret bleaching.

RESULTS

Preparation of H93G(Im-X) Adducts. Screening of a very wide range of N-heterocyles, including imidazoles and pyridines (not shown), for the ability to form six-coordinate high-spin aquo species led to the choice of five imidazoles which are listed in Figure 1. The choice of these series of ligands was based on their ability to form the required imidazole−aquo complex with H93G at low concentrations.

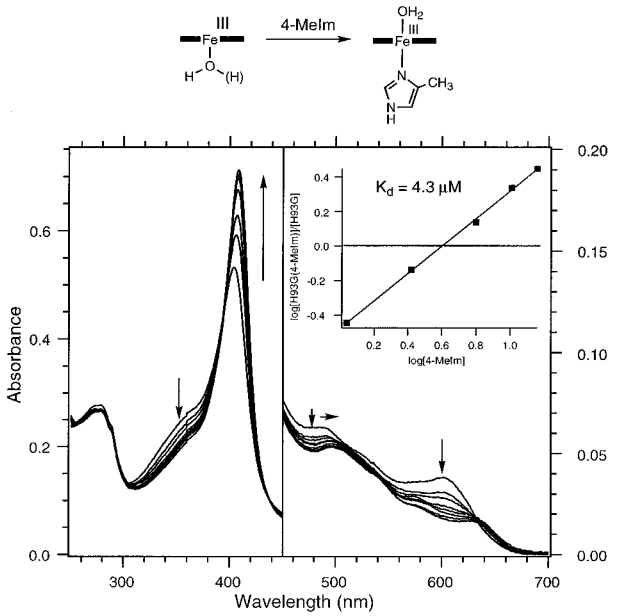

FIGURE 2: UV−visible spectra of the titration of 5 μM exogenous ligand free ferric H93G in 50 mM phosphate buffer (pH 7.0) with 4-MeIm (in DMSO) at 25 °C. The Hill plot used to calculate the dissociation constant is shown in the inset.

Though pyridine and 3-fluoropyridine adducts of ferrous−CO H93G have been reported (*22*), under the conditions employed here these ligands were found to form less well-defined complexes with exogenous ligand free ferric H93G as judged from UV−visible spectra (not shown). Other examples of substituted imidazoles and pyridines either bound poorly, formed unusual low-spin species, or had significant contaminating absorbance in the spectral region of interest (e.g., nitro-substituted imidazoles) (data not shown).

A representative example of an Im-X titration and a K_d determination are displayed in Figure 2. As 4-MeIm is added to a solution of 5 μM exogenous ligand free ferric H93G, the Soret band experiences an intensity increase and shifts from 405 to 409 nm. Further changes are evident in the visible region of the spectrum where the broad charge-transfer band at 602 nm experiences an intensity decrease and shifts to 630 nm. In addition, the maximum at 476 nm decreases and undergoes a red shift to 500 nm. The similarity of the final spectrum with that of wild-type ferric myoglobin (not shown) is evidence that a six-coordinate high-spin aquo−imidazole coordination structure has been attained. Hill analysis of these data (Figure 2 inset) indicates that the K_d of 4-MeIm is 4.3 μM (average). The tight binding of 4-MeIm and the spectral similarity of ferric H93G(4-MeIm) to ferric wild-type myoglobin indicate that the H93G(4-MeIm) complex is suitable for further investigations of reactions with peroxides. Likewise, 2-MeIm, 1-MeIm, Im, and 1-VinylIm adducts of H93G were deemed suitable for further study (data not shown). The K_d values of the five Im-X compounds are listed in Table 1. Of these five Im-X compounds, four have K_d values on the same order of magnitude. The fifth, 2-MeIm, has a K_d that is 1 order of magnitude higher than the others. The variable ligand binding characteristics have been normalized for each H93G(Im-X) adduct by preparing ligand concentrations that are 10-fold higher than the K_d in each different H93G(Im-X) solution.

Reactions of H93G(Im-X) with H_2O_2. Rapid scan stopped flow spectra obtained during the course of the reaction of H93G(Im) with 100 mM H_2O_2 are displayed in Figure 3. The shift of the Soret band from 409 nm to about 419 nm and the rise of visible bands at about 540 and 580 nm as well as a good fit to a single exponential equation indicate that a relatively stable oxo-ferryl complex is formed in the reaction. The observed rate of formation (k_{obs}) of H93G-(Im)-II in this case is 3.92 s^{-1}. Similarly, H93G-II k_{obs} were determined for the other four H93G(Im-X) adducts at a range of concentrations of H_2O_2 between 30 and 120 mM.

In Figure 4, a plot of k_{obs} vs H_2O_2 concentration for each H93G(Im-X) is shown. For each H93G(Im-X) the plot yields a straight line whose slopes are equivalent to H93G(Im-X)-II k_{app}, the apparent rate of formation of each H93G(Im-X)-II. H93G(Im-X)-II k_{app} is clearly dependent on the identity of each Im-X. H93G(Im-X)-II k_{app} values are listed in Table 1 and show a strong correlation with the N-3 pK_a of each Im-X (Table 1).

Measurement of Association Rates of H93G(Im-X) with NaN_3. Because the formation of Mb-II upon reaction with H_2O_2 involves several steps (Scheme 1), it was of interest to investigate whether the Im-X ligands have an influence on the simple binding of a sixth ligand trans to the Im-X. If an associative trans effect existed, it would indicate that the dependence of H93G(Im-X)-II k_{app} on Im-X N-3 pK_a is not necessarily a manifestation of a push effect but possibly due to a simple binding effect. On the other hand, if a repulsive trans effect existed, it might lead to some precatalytic masking of the O−O bond cleavage step so that the actual influence of N-3 pK_a is actually greater than it appears. To investigate this premise, azide was chosen as a sixth ligand probe because its binding mode (primarily σ-bonding interactions with negligible π-back-bonding) should be a close approximation of that of HO_2^- (singly deprotonated H_2O_2). In addition, no N−N bond cleavage is involved. Rapid scan stopped flow spectra obtained during the course of the reaction of H93G(Im) with 10 mM NaN_3 are displayed in Figure 5. The shift of the Soret band from 409 to ∼420 nm and the rise of visible bands at ∼536 and ∼575 nm as well as a good fit to a single-exponential equation indicate that a stable azide adduct is formed. The observed rate of formation (k_{obs}) of H93G(Im)-N_3^- in this case is 6.77 s^{-1}. Similarly, H93G-N_3^- k_{obs} values were determined for the other four H93G(Im-X) adducts at a range of concentrations of NaN_3 between 1 and 15 mM.

In Figure 6, a plot of k_{obs} versus NaN_3 concentration for each H93G(Im-X) is shown. As in Figure 4, each plot yields a straight line whose slopes are equivalent to H93G(Im-X)-N_3^- k_{app}, the apparent rate of formation of each H93G(Im-X)-N_3^-. The data show significant variation depending on the identity of Im-X. However, unlike the data obtained for H93G(Im-X)-II k_{app}, there appears to be no direct dependence of H93G(Im-X)-N_3^- k_{app} on the Im-X N-3 pK_a (Table 1).

The H93G(Im-X)-II k_{app} data and the H93G(Im-X)-N_3^- k_{app} data are compared more directly in Figure 7. Since there is an ∼1 order of magnitude separation between the two different sets of k_{app} data, they have been plotted on two separate log axes on the same scale versus the N-3 pK_a for each Im-X. It is readily apparent that a strong correlation exists between H93G(Im-X)-II k_{app} and the pK_a of each Im-X proximal ligand. Essentially no such correlation exists for

Table 1: Substituted Imidazole N-3 pK_a Values, Dissociation Constants for Binding to H93G, and Rate Data for H93G(Im-X) Reactions with H_2O_2, NaN_3, Peracetic Acid, and Cumene Hydroperoxide

ligand (Im-X)	N-3 pK_a	K_d[a]	H93G(Im-X)-II K_{app}[b]	H93G-N_3 K_{app}[c]	PAA k_{1obs}[d]	CHP k_{1obs}[e]
2-MeIm	7.92	680	5.1 ± 0.3	4.1 ± 0.1	0.93 ± 0.01	0.19 ± 0.01
4-MeIm	7.57	4.3	4.7 ± 0.3	6.5 ± 0.1	0.33 ± 0.01	0.14 ± 0.01
1-MeIm	7.02	48	3.1 ± 0.2	8.3 ± 0.4	1.10 ± 0.04	0.14 ± 0.02
Im	7.01	10	3.8 ± 0.3	4.4 ± 0.2	0.74 ± 0.01	0.09 ± 0.01
1-VinylIm	5.69	16	1.3 ± 0.1	5.9 ± 0.2	1.38 ± 0.05	0.11 ± 0.00
His93 (wild-type Mb)	−	−	4.7 ± 0.3	5.5 ± 0.1	ND[f]	ND[f]

[a] Dissociation constant for Im-X binding to exogenous ligand free ferric H93G (mM). [b] Apparent rate of formation of H93G(Im-X)-II (compound II) upon reaction with H_2O_2 ($\times 10^{-2}$ mM^{-1} s^{-1}). [c] Apparent rate of formation of the azide adduct of H93G(Im-X) upon reaction with NaN_3 ($\times 10^{-1}$ mM^{-1} s^{-1}). [d] Observed rate of the first phase of bleaching of the Soret band at 409 nm of H93G(Im-X) upon reaction with 1 mM PAA (s^{-1}). [e] Observed rate of the first phase of bleaching of the Soret band at 409 nm of H93G(Im-X) upon reaction with 1 mM CHP (s^{-1}). [f] Not determined.

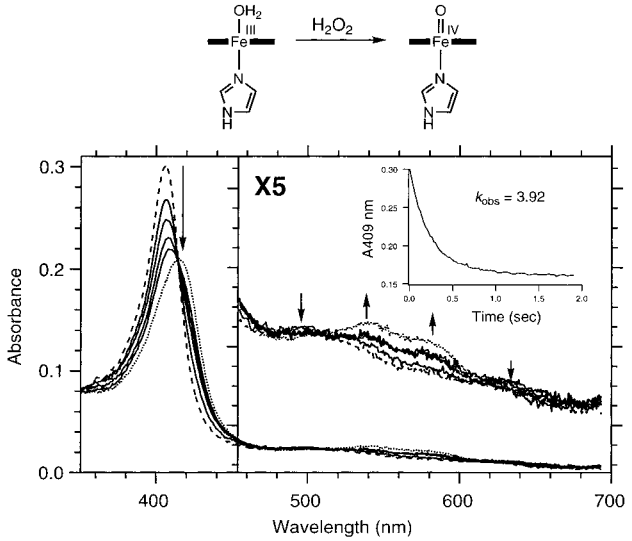

FIGURE 3: UV−visible rapid scan stopped flow reaction profile for the reaction of ferric H93G(Im) with H_2O_2. H93G (5 μM) and 100 μM imidazole in 50 mM potassium phosphate and 2% DMSO (pH 7.0) were mixed in a 1:1 ratio with 100 mM H_2O_2 in 50 mM potassium phosphate buffer (pH 7.0) at 4 °C: (− − −) the first spectrum immediately after mixing and (- - -) the spectrum 1.96 s after mixing. The decrease in absorbance at 409 nm is shown in the inset.

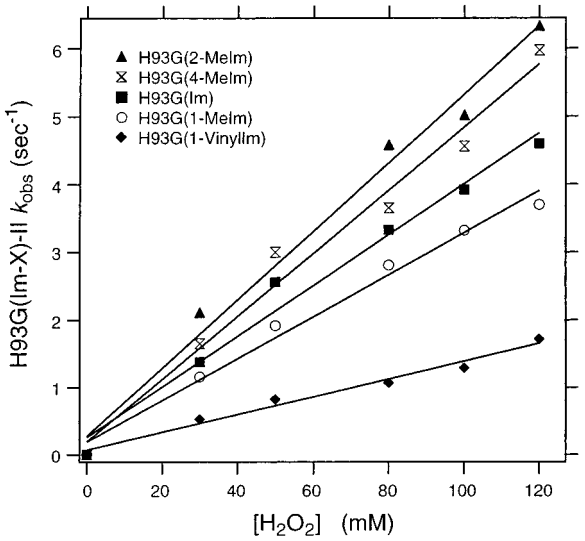

FIGURE 4: Plot of H93G(Im-X)-II k_{obs} vs H_2O_2 concentration for the five H93G(Im-X) adducts: (▲) H93G(2-MeIm), (double triangle) H93G(4-MeIm), (■) H93G(Im), (○) H93G(1-MeIm), and (◆) H93G(1-VinylIm).

the H93G(Im-X)-N_3^- k_{app} data set. This indicates that significant trans effects are not responsible for the H93G-(Im-X)-II k_{app} correlation with N-3 pK_a.

As shown in Scheme 1, the reaction of Mb with H_2O_2 leads to partitioning into heterolysis and homolysis after formation of the highly unstable ferric−peroxy intermediate. To simplify this reaction and make it a better model for peroxidase chemistry, it is desirable to channel the reaction exclusively to heterolytic cleavage. This can be done by employing peracids in place of H_2O_2. A rapid scan stopped flow spectrum of the reaction of H93G(2-MeIm) with 1 mM peracetic acid (PAA) from 0 to 2.8 s is displayed in Figure 8 as a representative example. It is readily obvious from the large decrease in absorbance of the Soret band that a significant amount of heme degradation (bleaching) has occurred. In addition to Soret bleaching, a red-shifted Soret band and the appearance of visible bands at ∼540 and ∼580 nm provide evidence of formation of a small fraction of compound II.

The decreases in absorbance at 409 nm have been fitted to a two-exponential equation (indicating a two-phase reaction in all cases) whose decay curves are shown in Figure 9. In addition, a list of PAA-dependent bleaching rates (PAA k_{1obs}) is given in Table 1. There appears to be no direct dependence of the PAA k_{1obs} on Im-X N-3 pK_a; however, the two smallest PAA k_{1obs} values are observed for H93G-(4-MeIm) and H93G(Im). These are the H93G adducts of the two Im-X species with the strongest binding constants (Table 1). Because of the complicated nature of the reactions of PAA with H93G(Im-X) and the failure to observe stable H93G-II species, we have not pursued further investigations of PAA reactions.

Stopped flow reactions of H93G(Im-X) with 1 mM cumene hydroperoxide (CHP) have been carried out in a manner similar to that of the PAA reaction set. Again, Soret bleaching was observed but without evidence of H93G-II formation and at slower rates (Table 1). As observed for PAA k_{1obs}, there is no direct dependence of the CHP k_{1obs} on the Im-X N-3 pK_a.

Recently, compound I of myoglobin (Mb-I) has been observed for the first time in mutants of myoglobin whose distal histidine has been either relocated or eliminated (*28*−*31*). Among these myoglobin mutants, H64D is able to react directly with H_2O_2 to form a Mb-I species which can be detected by rapid scan stopped flow spectroscopy (*31*). We prepared the double mutant H64D/H93G so we could directly observe H93G(Im-X) compound I species resulting from reactions with H_2O_2. The titration of exogenous ligand free

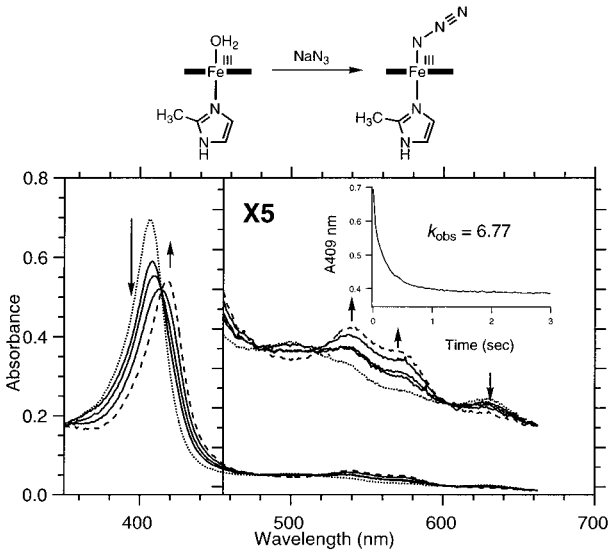

FIGURE 5: UV−visible rapid scan stopped flow reaction profile for the reaction of ferric H93G(2-MeIm) with NaN_3. H93G (10 μM) and 6.8 mM 2-MeIm in 50 mM potassium phosphate (pH 7.0) were mixed in a 1:1 ratio with 10 mM NaN_3 in 50 mM potassium phosphate buffer (pH 7.0) at 4 °C: (- - -) the first spectrum immediately after mixing and (− − −) the spectrum 1.96 s after mixing. The decrease in absorbance at 409 nm is shown in the inset.

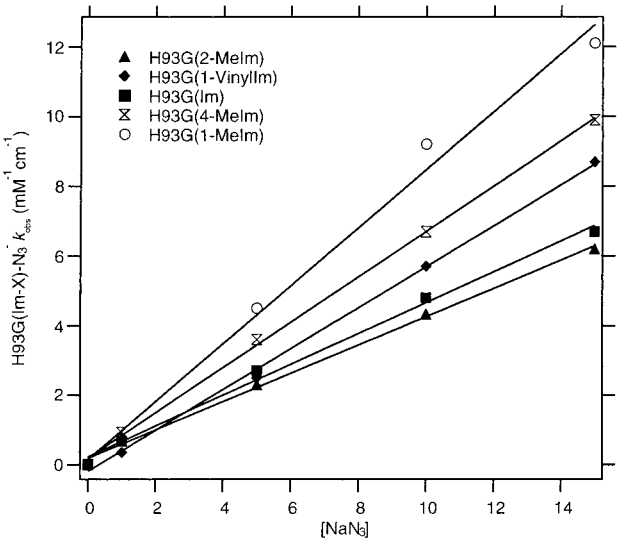

FIGURE 6: Plot of H93G(Im-X)-N_3 k_{obs} vs NaN_3 concentration for the five H93G(Im-X) adducts: (▲) H93G(2-MeIm), (double triangle) H93G(4-MeIm), (■) H93G(Im), (○) H93G(1-MeIm), and (◆) H93G(1-VinylIm).

ferric H64D/H93G with Im is shown in Figure 10. The isosbestic shift of the Soret band from 403 to 415 nm and the rise of visible bands at 536 and 565 nm indicate a direct transition from the exogenous ligand free state to a six-coordinate low-spin bis-Im complex whose K_d (for both ligands) is 12 μM. This is similar to the K_d for binding of a single Im to the single mutant H93G (10 μM). In addition, this complex was found to be resistant to reaction with H_2O_2 (data not shown).

DISCUSSION

The ligands chosen for the H93G modular peroxide O−O bond cleavage model system include 2-MeIm, 4-MeIm, 1-MeIm, Im, and 1-VinylIm. This series has the advantage

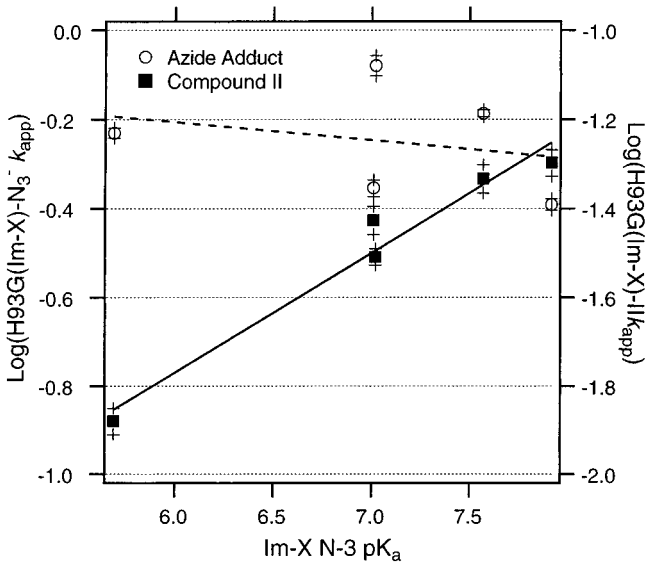

FIGURE 7: Plot of log[H93G(Im-X) k_{app}] (right axis) and log[H93G-(Im-X)-II k_{app}] (left axis) vs N-3 pK_a for all five Im-X species: (○) H93G(Im-X)-N_3^- k_{app} and (■) H93G(Im-X)-II k_{app}.

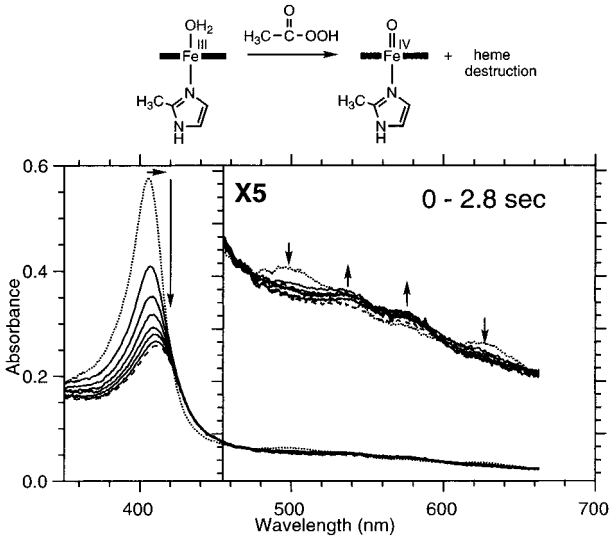

FIGURE 8: UV−visible rapid scan stopped flow reaction profile for the reaction of ferric H93G(2-MeIm) with 1 mM PAA. H93G (10 μM) and 6.8 mM 2-MeIm in 50 mM potassium phosphate (pH 7.0) were mixed in a 1:1 ratio with 1 mM PAA in 50 mM potassium phosphate buffer (pH 7.0) at 4 °C: (- - -) the first spectrum immediately after mixing and (− − −) the spectrum 2.8 s after mixing.

of having an Im-X N-3 pK_a range of 5.69−7.92, a total range of 2.23 pK_a units. The N-3 pK_a value is an indicator of the localization of electron density in the N-3 nonbonding σ-orbital and thus provides a means of directly comparing the electron donor ability of N-3 for this series of Im-X species. All of the ferric H93G(Im-X) complexes prepared with these ligands have six-coordinate aquo−imidazole coordination structures similar to that of wild-type Mb.

These Im-X species exhibit a range of binding affinities as well but all within the same order of magnitude except for that of 2-MeIm which is approximately 1 order of magnitude higher, indicating much weaker binding. These binding affinities follow the same qualitative trends observed for binding of imidazoles to H93G ferric−cyanide complexes (*21*) and ferrous−nitric oxide complexes (*23*).

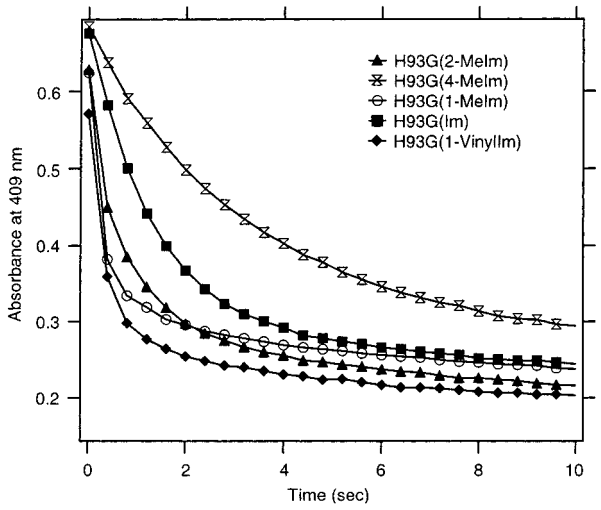

FIGURE 9: Plot of the Soret decay at 409 nm vs time for the reaction of ferric H93G(Im-X) with 1 mM PAA. H93G (10 μM) and Im-X (each at 10K_d) in 50 mM potassium phosphate (pH 7.0) were mixed in a1:1 ratio with 1 mM PAA in 50 mM potassium phosphate buffer (pH 7.0) at 4 °C: (▲) H93G(2-MeIm), (double triangle) H93G(4-MeIm), (■) H93G(Im), (○) H93G(1-MeIm), and (◆) H93G(1-VinylIm).

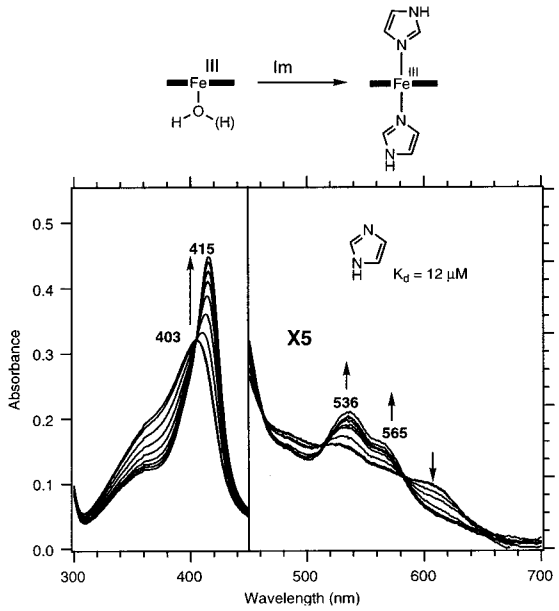

FIGURE 10: UV−visible spectra of the titration of approximately 3 μM exogenous ligand free ferric H64D/H93G in 50 mM phosphate buffer (pH 7.0) with 4-MeIm (in DMSO) at 25 °C.

In reactions of ferric H93G(Im-X) with H_2O_2, the variable ligand binding characteristics were normalized by keeping a constant concentration of each Im-X that was 10-fold higher than its K_d. When the data are compared with the reactivity of wild-type Mb with H_2O_2 (Table 1), it becomes evident that 4-MeIm is the exogenous ligand best suited to mimic the natural histidine 93 ligand of wild-type Mb. The functional similarity of histidine and 4-MeIm has already been predicted by Goodin (*3*). In addition, comparisons between the imidazole and 1-methylimidazole H93G complexes allow an assessment of the importance of the His93 N-1 hydrogen bond interactions in producing a partially ionized imidazolate ligand. The N-3 of imidazole and 1-methylimidazole have similar pK_as, and their H93G complexes have similar rates of reaction with H_2O_2. If blocking these hydrogen bonding interactions by using the 1-methylimidazole ligand were to disrupt the hydrogen bonds that lead to increased imidazolate character, evidence of a greatly decreased push effect should be observed relative to the imidazole ligand. The very modest difference observed between the push effect of H93G(Im) and H93G(1-MeIm) supports our current understanding whereby the His93 proximal ligand in Mb is predominately neutral (*32*) and the hydrogen bonding interactions observed at N-1 of His93 are primarily for structure stabilization and not for producing a partially ionized proximal ligand with an enhanced push effect (*33*). The preceding discussion indicates that the model system can provide a comparative assessment of the properties of a natural proximal ligand and its interactions with the surrounding protein environment through comparison with a series of unnatural ligands.

We have found that as the pK_a of the imidazole N-3 is increased, the reactivity with H_2O_2 as indicated by the apparent rate of formation of compound II [H93G(Im-X)-II k_{app}] is also increased (Figure 7). Over the entire range of 2.23 pK_a units from 1-vinylimidazole (pK_a = 5.69) to 2-methylimidazole (pK_a = 7.92), the reactivity of the complex increases by a factor of 3.7. However, since the reaction of Mb with H_2O_2 to produce Mb-II is known to be quite complex (Scheme 1), it was necessary to investigate whether the Im-X series is able to influence the simple binding of a sixth ligand through either associative or repulsive trans effects. N_3^- was chosen as a sixth ligand probe. Figure 7 indicates that while there is a significant variation in the H93G(Im-X)-N_3^- k_{app} data, there is essentially no dependence of the data on Im-X N-3 pK_a. The reason for the variation in the H93G(Im-X)-N_3^- k_{app} data is not known at this time. However, there is no evidence for significant Im-X N-3 pK_a trans effects. Therefore, the correlation of the H93G(Im-X)-II k_{app} data with Im-X N-3 pK_a may be taken as a direct effect of the electron donor characteristics of the proximal ligand on the cleavage of the O−O bond of heme iron-bound peroxide, an increase in the H93G(Im-X)-II k_{app} of 1.7-fold per pK_a unit.

In light of recent Mb mutagenesis studies which have indicated that changing the identity and/or position of distal basic residues in sperm whale Mb can cause dramatic increases in its reactivity with H_2O_2 (*28*, *29*, *31*, *34*), this relatively modest effect seems to indicate that, while varying the electron donor capability for an imidazole proximal ligand produces a visible change in the push effect, its mechanistic influence in the activation of peroxide is almost certainly not as strong as the pull effect from properly positioned distal catalytic residues. These combined observations may indicate that the primary role of the partial imidazolate proximal ligand of peroxidases is not to produce a mechanistically critical push effect. On the other hand, a hypothesis which has received some support lately is one in which the partial imidazolate ligand serves to stabilize compound I by modulating the redox potential of the heme complex (*3*, *4*, *35*). Unfortunately, the effect of compound I stability cannot be tested in H93G because of an inability to observe compound I directly (Scheme 1).

The results obtained to this point indicate that the Im-X N-3 pK_a directly affects the rate of H93G(Im-X)-II formation but do not give us specific information about the distribution of partitioning of the O−O bond cleavage step. In the next

reaction series, PAA was chosen as the oxidant because of its small size, its solubility in aqueous buffers, and its ability to channel the O−O bond cleavage mechanism to heterolysis. As an example, the rapid scan stopped flow reaction of H93G(2-MeIm) is shown in Figure 8. Unfortunately, a clean first-order transition to H93G(Im-X)-II was not observed. Instead, Soret bleaching, an indicator of heme destruction, was observed along with evidence of compound II formation. Although it is not observed, an unusually reactive compound I species formed as a result of Im-X displacement may be at least partially responsible for heme destruction. In reactions of PAA with all H93G(Im-X) species, the first phase of the reaction (PAA k_{1obs}) showed some variation with Im-X N-3 pK_a but no direct correlation (Figure 9 and Table 1). Instead, 4-MeIm and Im, the two Im-X species with the strongest binding affinities (4.3 and 10 μM, respectively), were found to exhibit the smallest PAA k_{1obs} (Figure 9 and Table 1). The reaction of exogenous ligand free ferric H93G has also been observed to yield rapid heme degradation (data not shown). Exogenous ligand free ferric H93G is composed of a mixture of bis-aquo and five-coordinate hydroxo structures (*27*, *36*). These observations of heme degradation upon reaction of H93G(Im-X) with PAA may indicate that Im-X dissociates in early stages of the reaction and that the resulting species lacking Im-X reacts rapidly with PAA to cause heme destruction. The tight binding of 4-MeIm and Im would be expected to reduce their rate of dissociation from H93G and lead to the slower rates of heme degradation. Further studies of the reactivity of exogenous ligand free H93G are now underway in our laboratory.

Cumene hydroperoxide (CHP) is often used in peroxide activation studies of heme complexes as a probe of the partitioning of O−O bond cleavage between heterolysis and homolysis (*9*). Preliminary data obtained from an HPLC-based assay of CHP reactions with H93G(Im-X) did not indicate a dependence of preferential heterolytic cleavage on Im-X N-3 pK_a (data not shown). Stopped flow experiments have been carried out in a manner similar to that of the PAA reaction set. Again, Soret bleaching was observed but at slower rates than those observed for the PAA reactions (Table 1) and without evidence of H93G-II formation. As observed for PAA k_{1obs}, there is no direct dependence of the CHP k_{1obs} on the Im-X N-3 pK_a.

The preceding results indicate that peracids and alkyl hydroperoxides are not suitable oxidants for use with the H93G O−O bond cleavage model system. H_2O_2 alone may be used as a H93G(Im-X)-II generating oxidant, and still leaves the problem of identifying whether the rate of heterolytic O−O bond cleavage is selectively altered by altering the electron donor properties of Im-X. This has prompted us to use a different strategy for which the double mutant H64D/H93G has been constructed. Recently, the single mutant H64D was found to be capable of reacting directly with H_2O_2 to form a compound I species (oxo−ferryl porphyrin cation radical) which could be detected by rapid scan stopped flow (*31*). Unfortunately, the exogenous ligand free ferric double mutant H64D/H93G was found to simultaneously bind imidazole to both axial positions to form a bis-imidazole complex (Figure 10). Subsequently, this H93G(Im)$_2$ species was found to be resistant to reaction with H_2O_2 (data not shown). It appears that the substitution of the distal histidine 64 with aspartate has opened up the distal heme cavity to an extent that imidazole is able to enter and bind to the heme iron even at very low concentrations. At the same time, this result has underscored an important feature of the H93G system; the presence of His64 prevents binding of imidazole at low concentrations so that the mixed ligand ferric aquo/Im-X coordination state analogous to the coordination structure of ferric wild-type Mb can be modeled accurately and that other mixed ligand adducts can also be formed (*25*).

CONCLUSIONS

The modular peroxide O−O bond cleavage model system consisting of substituted imidazole adducts of the myoglobin cavity mutant H93G is capable of altering the apparent rates of formation of compound II upon reaction with H_2O_2 in a manner directly dependent on the identity of the substituted imidazole ligand. Substituted imidazoles with high pK_a values and electron rich nonbonding σ N-3 orbitals accelerate the rate of formation of compound II. The binding of azide is not influenced by the identity of the substituted imidazole ligand in a similar manner, indicating that the increases in the rate of compound II formation are most likely not due to a simple binding effect but to the subsequent O−O bond cleavage steps. While the effects of altering the electron donor properties at N-3 of the substituted imidazoles are obvious, their overall influence on the apparent rates of formation of compound II are quite modest (a 1.7-fold increase per N-3 pK_a unit increase). This could be an indicator that the partially ionized proximal imidazolate ligand of peroxidases does not contribute significantly to the fast rates of selective O−O bond heterolysis. The inability to observe a stable compound II upon reactions of the model system with peracetic acid and cumene hydroperoxide has prevented us from drawing conclusions regarding the manner in which the substituted imidazoles influence the relative amounts of O−O bond heterolysis and homolysis. The latter investigations have indicated that the advantage of being able to carry out convenient exchanges of ligands in the proximal pocket of H93G can turn into a disadvantage when the oxidants employed to generate high-valent intermediates are themselves capable of displacing the original ligand. Finally, His64 appears to provide a crucial steric effect which prevents access of exogenous ligands to the distal binding site at low concentrations and thus allows mixed ligand adducts of H93G(Im) to be prepared (*25*).

ACKNOWLEDGMENT

We thank Dr. John S. Olson (Rice University) for providing cDNA of sperm whale myoglobin and Drs. Toshitaka Matsui and Yoshio Goto for helpful discussions. M.P.R. thanks Prof. Steven G. Boxer and Prof. John H. Dawson for the initial opportunity to study sperm whale myoglobin H93G.

REFERENCES

1. Watanabe, Y. (1997) in *Oxygenases and Model Systems* (Funabiki, T., Ed.) pp 223−282, Kluwer, Dordrecht, The Netherlands.
2. Sono, M., Roach, M. P., Coulter, E. D., and Dawson, J. H. (1996) *Chem. Rev. 96*, 2841−2887.
3. Goodin, D. B. (1996) *JBIC, J. Biol. Inorg. Chem. 1*, 360−363.

4. Poulos, T. L. (1996) *JBIC, J. Biol. Inorg. Chem. 1*, 356−359.
5. Groves, J. T., and Han, Y.-Z. (1995) in *Cytochrome P450 Structure, Mechanism and Biochemistry* (Ortiz de Montellano, P. R., Ed.) pp 3−48, Plenum, New York.
6. Dawson, J. H. (1988) *Science 240*, 433−439.
7. Poulos, T. L. (1988) *Adv. Inorg. Biochem. 7*, 1−36.
8. Adachi, S., Nagano, S., Watanabe, Y., Ishimori, K., and Morishima, I. (1991) *Biochem. Biophys. Res. Commun. 180*, 138−144.
9. Adachi, S., Nagano, S., Ishimori, K., Watanabe, Y., Morishima, I., Egawa, T., Kitagawa, T., and Makino, R. (1993) *Biochemistry 32*, 241−252.
10. Matsui, T., Nagano, S., Ishimori, K., Watanabe, Y., and Morishima, I. (1996) *Biochemistry 35*, 13118−13124.
11. Higuchi, T., Shimada, K., Maruyama, N., and Hirobe, M. (1993) *J. Am. Chem. Soc. 115*, 1551−1552.
12. Higuchi, T. (1996) *Keio J. Med. 45*, s66.
13. Yamaguchi, K., Watanabe, Y., and Morishima, I. (1993) *J. Am. Chem. Soc. 115*, 4058−4065.
14. Barrick, D. (1994) *Biochemistry 33*, 6546−6554.
15. Barrick, D. (1995) *Curr. Opin. Biotechnol. 6*, 411−418.
16. McRee, D. E., Jensen, G. M., Fitzgerald, M. M., Siegel, H. A., and Goodin, D. B. (1994) *Proc. Natl. Acad. Sci. U.S.A. 91*, 12847−12851.
17. Sun, J., Fitzgerald, M. M., Goodin, D. B., and Loehr, T. M. (1997) *J. Am. Chem. Soc. 119*, 2064−2065.
18. Sun, J., Loehr, T. M., Wilks, A., and Ortiz de Montellano, P. R. (1994) *Biochemistry 33*, 13734−13740.
19. Newmyer, S. L., Sun, J., Loehr, T. M., and Ortiz de Montellano, P. R. (1996) *Biochemistry 35*, 12788−12795.
20. DePillis, G. D., Decatur, S. M., Barrick, D., and Boxer, S. G. (1994) *J. Am. Chem. Soc. 116*, 6981−6982.
21. Decatur, S. M., and Boxer, S. G. (1995) *Biochemistry 34*, 2122−2129.
22. Decatur, S. M., DePillis, G. D., and Boxer, S. G. (1996) *Biochemistry 35*, 3925−3932.
23. Decatur, S. M., Franzen, S., DePillis, G. D., Dyer, R. B., Woodruff, W. H., and Boxer, S. G. (1996) *Biochemistry 35*, 4939−4944.
24. Roach, M. P., Franzen, S., Pang, P. S. H., Woodruff, W. H., Boxer, S. G., and Dawson, J. H. (1998) in *Oxygen Homeostasis and Its Dynamics* (Ishimura, Y., Shimada, H., and Suematsu, M., Eds.) pp 172−180, Springer-Verlag, Tokyo.
25. Roach, M. P., Pond, A. E., Thomas, M. R., Boxer, S. G., and Dawson, J. H. Manuscript in preparation.
26. Teale, W. (1959) *Biochim. Biophys. Acta 35*, 543−550.
27. Pond, A. E., Roach, M. P., Sono, M., Rux, A. H., Franzen, S., Hu, R., Thomas, M. R., Wilks, A., Dou, Y., Ikeda-Saito, M., Ortiz de Montellano, P. R., Woodruff, W. H., Boxer, S. G., and Dawson, J. H. (1999) *Biochemistry 38*, 7601−7608.
28. Ozaki, S., Matsui, T., and Watanabe, Y. (1996) *J. Am. Chem. Soc. 118*, 9784−9785.
29. Ozaki, S., Matsui, T., and Watanabe, Y. (1997) *J. Am. Chem. Soc. 119*, 6666−6667.
30. Matsui, T., Ozaki, S., and Watanabe, Y. (1997) *J. Biol. Chem. 272*, 32735−32738.
31. Matsui, T., Ozaki, S., and Watanabe, Y. (1999) *J. Am. Chem. Soc. 121*, 9952−9957.
32. Li, X.-Y., and Spiro, T. G. (1988) *J. Am. Chem. Soc. 110*, 6024−6033.
33. Peterson, E. S., Friedman, J. M., Chien, E. Y., and Sligar, S. G. (1998) *Biochemistry 37*, 12301−12319.
34. Matsui, T. (1997) PhD Thesis; Roles of Distal Residues in Catalytic Oxidation by Heme Enzymes in *Department of Structural Molecular Science*, Graduate University for Advanced Studies, Okazaki, Japan.
35. Smulevich, G., Neri, F., Willemsen, O., Choudhury, K., Marzocchi, M. P., and Poulos, T. L. (1995) *Biochemistry 34*, 13485−13490.
36. Das, T. K., Franzen, S., Pond, A., Dawson, J. H., and Rousseau, D. L. (1999) *Inorg. Chem. 38*, 1952−1953.

BI992054V